Comparative Dielectric Behavior of $PbFe_{1/2}Ta_{1/2}O_3$ and $NaNbO_3$:Gd Relaxor-Like Crystals

I. P. Raevski[1,2], S. A. Prosandeev[1,3], U. Waghmare [3,4], V. V. Eremkin[2] , V. G. Smotrakov[2] , V. A. Shuvaeva[2]

February 1, 2008

[1]Physics Department, Rostov State University, 344090 Rostov on Don, Russia

[2] Research Institute of Physics, Rostov State University, 344090 Rostov on Don, Russia

[3]Ceramics Division, A317/223, 100 Bureau Drive, STOP 8520, National Institute of Standards and Technology, Gaithersburg, MD

[4]Theoretical Sciences Unit, J Nehru Centre for Advanced, Scientific Research, Bangalore, India 560 064

Abstract

Experimental data obtained for $PbFe_{1/2}Ta_{1/2}O_3$ (PFT) and $NaNbO_3$: Gd (NaNbGd) single crystals show a diffused dielectric permittivity peak that is inherent to relaxor ferroelectrics. However some deviations from the normal relaxor properties were also observed and are under discussion. One of the key features of the relaxors is the existence of the Burns temperature, at which the polar regions appear. We found out that PFT shows this feature but the NaNbGd dielectric behavior is different. We analyse these properties within a phenomenological theory and propose a microscopic model.

1 Introduction

Relaxor properties of heterogeneous ferroelectrics are still intriguing although the main phenomenon, the diffuseness of the temperature dielectric-permittivity peak, was discovered long ago [1]. It is now established that one of the important features of relaxors is the polar-regions formation and these regions grow with decreasing temperature and reach their maximal sizes at the ferroelectric or glass-type phase transition [2].

New information, rather useful for understanding the relaxor properties, was recently obtained from neutron scattering which establishes the existence of a soft ferroelectric mode above the Burns temperature T_d, and below the freezing temperature $T_g (T_d > T_g)$, [3, 4]. In the intermediate temperature range, the "waterfall phenomenon" is seen [4] which reflects the absence of transverse optical mode below a definite wave vector. Another new idea stemmed from the diffuse scattering of neutrons in relaxors suggesting a uniform displacement of the ions in polar regions along with optical displacements [5]. We use these findings to establish the order parameter in the relaxor state.

The present study considers the dielectric behavior of $PbFe_{1/2}Ta_{1/2}O_3$ (PFT), and $NaNbO_3$:Gd (NaNbGd) crystals which have some common features (the diffuseness of the temperature dielectric peak) as well as some differences. In PFT, the extrapolated Curie-Weiss temperature, T_{CW}, is above the temperature of dielectric permittivity maximum, T_m, hinting that a ferroelectric phase transition would occur if the crystal were homogeneous. The heterogeneities in the crystal prevent the appearance of the ferroelectric phase and lead to changes in the temperature dependence of dielectric permittivity characteristic of the relaxor state below T_{CW} [1]. We connect these changes with the appearance of a new order parameter corresponding to a nanodomain structure and show an example of such a structure within a model considering a heterogeneous material consisting of slabs (for the sake of simplicity) having different elastic and dielectric properties. In contrast with PFT, we find that $T_{CW}$is lower than T_m and another order parameter appears at T_m in NaNbGd.

2 Experimental

$PbFe_{1/2}Ta_{1/2}O_3$(PFT), and $NaNbO_3$:Gd (NaNbGd) crystals were grown by the flux method. The crystals obtained had an isometric (edge dimensions 0.5 -2 mm) form with the sides parallel to the {100} planes of the perovskite prototype lattice. The details of the crystal preparation and characterization have been described elsewhere [6, 7].

The dielectric studies were carried out in the 10^3 -10^6Hz range in the course of both heating and cooling at the rate about 2 -3 K/min with the aid of the R5083 and E7-12 capacitance bridges. Aquadag electrodes for dielectric measurements were deposited on the opposite faces of the as-grown crystals.

3 $PbFe_{1/2}Ta_{1/2}O_3$

At high temperatures PFT has the cubic perovskite structure in which the B-perovskite-position is occupied by the approximately randomly distributed Fe^{3+} and Ta^{5+} ions. This random distribution influences the displacements of the Pb ions and can result in the appearance of polar clusters whose interactions and growths can trigger a phase transition into a glassy or ordered phase. Fig. 1 shows the real part of the dielectric permittivity of the PFT crystal measured at different frequencies in the 10^3 -10^6Hz range. The strong frequency dispersion of ε observed at temperatures well above T_d is likely to be due to conductivity [1]. In addition to the known $\varepsilon(T)$ curves for PFT crystals [8] and ceramics [1, 9], besides a diffused and frequency-dependent $\varepsilon(T)$ maximum typical of relaxors, an inflection is observed in the $\varepsilon(T)$ curve at temperature T_{ip}, which is 30-40 K lower then T_m. The frequency dispersion of ε is less pronounced at temperatures below this inflection than above it. Such behavior is similar to that observed in $PbSc_{1/2}Ta_{1/2}O_3$ and $PbSc_{1/2}Nb_{1/2}O_3$ [10] at the spontaneous transition from the relaxor to normal ferroelectric state (see also [11]), but for PFT, it can be also connected with a glass-type phase transition which appears due to percolation of polarization [12, 13], or antiferromagnetic phase transition [1, 8] (recent results on Rietveld refinement of the neutron diffraction data [14] does not show any symmetry changes in PFT from room temperature down to 10 K when the superstructure due to the antiferromagnetic ordering is taken into account).

The fit of the Curie-Weiss law to the high temperature side of the $\varepsilon(T)$

curve measured at a high frequency (Fig. 2) provides the extrapolated Curie-Weiss temperature $T_{CW} \approx 310$ K which is substantially higher than T_m. In the same figure we show the difference between the experimental $1/\varepsilon$ curve and the Curie-Weiss fit. It is seen that this difference has two portions where it behaves approximately linearly with temperature. One of the portions intersects the temperature axis at temperature T_η which approximately equals T_{CW}, while the other, seen at lower temperatures, intersects the T axis at a temperature which is close to the value $T_{VF} \approx 246$ K obtained from the Vogel-Fulcher fit of the T_m dependence on frequency.

The fact that $T_\eta \approx T_{CW}$ hints to identify a new order parameter appearing at this temperature with local polarization. It is consistent with the idea that in PFT, at some temperature, T_d, there appear polar regions (T_d is higher than T_{CW} because of the diffusness of the phase transition that we will discuss in detail in Section 5). At the same temperature the dielectric permittivity starts deviating from the Curie-Weiss law.

It was rigorously shown in Ref. [15] that, in the heterogeneous media consisting of a ferroelectric slab and dielectric layers (dead layers) the ferroelectric region gets broken into 180^0 domains in order to decrease the depolarization field (see Section 6 where we consider the rigorous solution for similar inhomogeneous problem: two ferroelectric slabs separated by dielectric interfacial layers). On this basis we propose the appearance of such (possibly short-range) randomly oriented domain structure in the relaxor state below T_d. We will discuss the consistency of this idea with other experiments in Section 7.

4 $NaNbO_3$:Gd

$NaNbO_3$ exhibits an antiferroelectric phase transition at 630^0 K [1, 16]. When being doped with Gd at small concentrations the temperature of this phase transition decreases and the width of the temperature hysteresis increases. We discussed these trends in Ref. [16] assuming the (1-x) $NaNbO_3$–(x)$Gd_{1/3}NbO_3$ solid solution formation. At $x \approx 0.12$ the thermal hysteresis abruptly disappears and a diffused hysteresis-free dielectric peak remains at higher concentrations (Fig. 3). We regarded this behavior in Ref. [16] to the appearance of a concentration phase transition into the relaxor-like state. However there are features which are different in comparison with ordinary relaxors.

First of all we find that that the T_{CW} found from the Curie-Weiss fit of the high-temperature side of the dielectric permittivity is much lower than T_m (Fig. 4). This makes scenario described in the previous section not suitable for the experimental data for NaNbGd and another scenario should be developed. In the next Section we will consider a reason for the diffusness of the phase transition. We will show that, in spite of the different meaning of the order parameter η for PFT and NaNbGd, the diffuseness of the dielectric permittivity peak in these two cases can have similar origin.

5 Landau-type theory of the diffuseness of the phase transitions in PFT and NaNbGd

In Ref. [16] we considered the strain and average square of local polarization as concomitant order parameters to an antiferroelectric order parameter. The addition of Gd results in the appearance of some distorted polar regions. The order parameter which is connected with these regions and responsible for the deviation from the Curie-Weiss behavior can have different meaning in different materials. For example, it can be the average square of polarization or local deformation or, if one thinks about the electronic subsystem, the degree of electron localization. In the case of PFT this order parameter can correspond to the magnitude of the local polarization in the nanodomain structure. In NaNbGd it can be an antiferroelectric order parameter. We use for this order parameter the notation η, we assume that it is scalar or a tensor of the second kind, which in the product with P^2 gives a scalar, and we write Landau Free energy expansion:

$$\begin{array}{l} F = F_0 + \frac{1}{2}\left(\alpha + qu\right)P^2 + \frac{1}{4}\beta P^4 + \frac{1}{6}\gamma P^6 + \frac{1}{2}\lambda P^2\eta + \\ + \frac{1}{2}A\eta^2 + \frac{1}{3}B\eta^3 - ku\eta + cu^2 - EP - (\sigma_0 + \sigma)u + ... \end{array} \quad (1)$$

where $\alpha = a(T - T_{CW})$, $A = b(T - T_\eta)$. Here $T_\eta \geq T_{CW}$; $u$is strain and σ_0 is internal stress (caused by Gd in the case of NaNbGd).

The equilibrium solutions for this Free energy are simple:

$$
\begin{aligned}
&1.\, P = 0,\ \eta = 0 \\
&2.\, P = 0,\ \eta = \frac{-A + \sqrt{A^2 + 4kuB}}{2B} \\
&3.\, \eta = \frac{-A + \sqrt{A^2 + 4B(ku + \lambda P^2)}}{2B}, \\
&P^2 = \frac{\alpha + qu + \lambda\eta \pm \sqrt{(\alpha + qu + \lambda\eta)^2 - 4\beta\gamma}}{2\gamma}
\end{aligned}
\tag{2}
$$

Here u is the strain found from the equilibrium condition (it is always finite because of the stress σ_0; the electrostriction contribution to the Hamiltonian quP^2 simply shifts the Curie-Weiss temperature and changes the value of the nonlinearity constant β). The first phase is stable at high temperatures. Then, at lower temperatures, the phase 2 becomes stable, with the order parameter η, and, at even lower temperatures, the third phase, where the ferrolectric order parameter (here we do not pay much attention to the difference between the glass-type and ferrolectric solutions as we are mostly interested in the relaxor state) coexists with the order parameter η. The values of η and P can be found from the solution of equations (11.3).

In order to find the dielectric permittivity one can write the equilibrium condition with respect to P:

$$
(\alpha + qu)\, P + \beta P^3 + \gamma P^5 + \lambda P\eta = E \tag{3}
$$

By taking the derivative of this equation with respect to E one can find

$$
\chi = \frac{1}{\varepsilon_0}\frac{\partial P}{\partial E} = \frac{1}{\varepsilon_0}\frac{1}{\alpha + qu + 3\beta P^2 + 5\gamma P^4 + \lambda\eta} \tag{4}
$$

For the phase (2) in (2) P =0 and $\lambda\eta = \lambda b\left(\sqrt{x^2 + \delta} - x\right)/2B$ where $x = (T - T_\eta)$, $\delta = 2ku/b$. In this case (4) takes the form

$$
\varepsilon = \frac{1}{\varepsilon_0}\frac{1}{\alpha + qu + \lambda b\left(\sqrt{x^2 + \delta} - x\right)/2B} \tag{5}
$$

From experimental data we found $\varepsilon_0\lambda\eta$ which is simply the difference between $1/\varepsilon$ and the high temperature Curie-Weiss dependence $(1/\varepsilon)_{CW} =$

$\varepsilon_0(\alpha + qu)$. A fit of the expression $\varepsilon_0\lambda\eta = \varepsilon_0\lambda b\left(\sqrt{x^2+\delta} - x\right)/2B$ to the experimentally obtained $1/\varepsilon - (1/\varepsilon)_{CW}$ for NaNbGd is shown in Fig. 5 (Notice that the same quality fit and the same results were obtained from the fit of (5) to the corresponding experimental curve). We find that this fit obtained with $\varepsilon_0 a = 3.2861 \cdot 10^{-6} \pm 3.78 \cdot 10^{-9}$, $T_{CW} = 185.75 \pm 1.84$ K, $\varepsilon_0\lambda b/2B = 3.91 \cdot 10^{-6} \pm 3 \cdot 10^{-8}$ K^{-1}, $T_\eta = 308.4 \pm 0.6$ K and $\delta = 1084.4 \pm 54$ K^2 is rather good and explains the deviation of the dielectric permittivty from the Curie-Weiss law by the appearance of the new order parameter below T_η and by the existence of local stresses. We have obtained a similar good fit for PFT (Fig. 5) at the values: $\varepsilon_0\lambda b/2B = 7.16 \cdot 10^{-6} \pm 1.2 \cdot 10^{-7}$ K^{-1}, $T_\eta = T_{CW} = 295.6 \pm 1.0$ K and $\delta = 1450.6 \pm 80$ K^2. From these data the appearance of the quadratic temperature dependencies of $\varepsilon(T)$ at the maximal position becomes clear: it appears due to the expansion of the square root in expression (3) with respect to x for small x. Hence we regard the diffuseness of the temperature maximum of the dielectric permittivity in NaNbGd to local quenched stresses and fields produced by the Gd impurities in the matrix of $NaNbO_3$ and local polar fields produced by the random distribution of Fe and Ta at the B-sites in PFT.

6 A model for structural inhomogeneity

We propose a model for structural inhomogeneity based on the recent finding by Bratkovskiy and Levanyuk [15] who studied a short-circuited ferroelectric slab with dead layers. Consider short-circuited ferroelectric slabs of the width f(for the sake of simplicity we consider two slabs) divided by dielectric interfacial layers with the width d_0 at the boundaries of the whole system (were the system has metalic contacts) and with the width d in the middle (see Fig. 6).

We show that the strain can be excluded from the equations by the ordinary minimization procedure. Let us consider the term describing the electrostriction effect together with the corresponding elastic contribution: $H_{elast}(r) = c_{\alpha\beta\alpha\beta}u^2_{\alpha\beta}/2 - q_{zz\alpha\beta}u_{\alpha\beta}P_zP_z$ where $u_{\alpha\beta}(r)$ is a component of the strain and $P_z(r)$ is a component of local polarization (at finite values of the local polarization one may consider a piezoelectric effect instead of the electrostriction one taking into account that $(P_s + \delta P)^2 \approx P_s^2 + 2P_s\delta P$). Minimizing this Hamiltonian with respect to the strain component one immediately obtains: $u_{\alpha\beta} = q_{zz\alpha\beta}P_zP_z/c_{\alpha\beta\alpha\beta}$ (at finite local polarizations $u_{\alpha\beta} =$

$d_{z\alpha\beta}P_z/c_{\alpha\beta\alpha\beta}$ where $d$is a piezoelectric coefficient depending on the direction of the local polarization). It implies that the strain can be excluded from the total Hamiltonian for problems with zero or constant stress. Then, we look for a lowest energy solution with possible spatial alternation of polarization for ferroelectrics which are improper ferroelastics. Detailed solution is worked out in Appendix A.

The macroscopic field energy (see Appendix, expression (A8)) is represented in the form

$$f_M = F_M/LS = f_{M0} + \tfrac{1}{2}A\sigma_0^2 - E^*\sigma_0 \tag{6}$$

where σ_0 is the average charge on the ferroelectric-dielectric boundary; the coefficients are given in Appendix A. The effective field E^* differs from the average field $E = U/\varepsilon_t L$ by the factor $2\varepsilon_t^2 f/\varepsilon_{2z}L$ where U is applied voltage, ε_t is the total dielectric permittivity obtained treating the system as a series of the capacitors, ε_{2z} is the dielectric permittivity of the ferroelectric slab. This factor is small only when f(thickness of the ferroelectric clab) is very small. This fact implies that the effective acting field E^* conjugated with σ_0 for the thick ferroelectric layers and thin dielectric interfacial layers is largely enhanced with respect to the average field that makes it possible to change the polarization by very small dc fields.

On the basis of these results we predict the appearance of the alternating domains in the ferroelectric slabs separated by dielectric layers in lamellar structures. Perhaps some evidence for this was found in the $KTaO_3/KNbO_3$ superstructure [17] although this has not been understood well yet.

The equilibrium value of the macroscopic charge at the boundaries σ_0 corresponds to the minimum of the macroscopic Free energy: $\sigma_0 = U\varepsilon_8/8\pi L_g$ (ε_g is the dielectric permittivity of the capacitors corresponding only to the dielectric interfacial layers, L_g is the total width of the dielectric layers along thefield). Correspondingly, the derivative of this charge with respect to field gives

$$\frac{d\sigma_0}{dE} = \frac{L\varepsilon_g}{8\pi L_g} \tag{7}$$

It is seen that this derivative is large if the total relative length of the dielectric interfacial layers L_g/L is small. This result is consistent with that

obtained in [15] for one ferroelectric slab having dead layers. There can be some variations of the dielectric region's widths but only their total relative width is important. We point out that this contribution to the dielectric permittivity arises only from the domain walls movements due to the voltage Uwhich results in change in total polarization, hence on σ_0.

We now relate the stripe-like solution to experimentally observable quantities. For a given solution of local polarization, we obtain local strains through the minimization of energy with respect to local strain [34] as described at the beginning of this section. The local strains are then used to obtain the acoustic-like (collective motions of atoms in the unit cell) atomic displacements $d_\alpha(r)$ through the relation: $u_{\alpha\beta} = \frac{1}{2}\left(\frac{\partial d_\alpha}{\partial r_\beta} + \frac{\partial d_\beta}{\partial r_\alpha}\right)$. For simplicity, we restrict here to analysis in 2 dimensions.

In addition to the solution with polarization in the domain perpendicular to the plane of the strip (the transverse case T) described in this section, we consider a longitudinal (L) case where the polarization is in the plane of stripe and along the direction perpendicular to the domain wall. Note that the polarization in the adjacent domains is opposite in sign, giving 180^0-type domain walls separating them. The polarization is along (1-1) and (-11) directions for the transverse case and along (2) and (-1-1) directions in the longitudinal case, and the strip itself runs along (2) direction. In Figure 7, we show contourplots of atomic displacements, local strains and local polarization for the two cases. It is clear that the atomic displacements in the transverse case are almost constant at the boundaries between polar domains and the embedding dielectric. In contrast, we find large accumulated local strains at the domain walls for the longitudinal case, making it costly in energy.

We use atomic displacements d_α(acoustic modes) and polarization P_α(optical modes) in Eq. (2) of [13] to obtain inelastic scattering intensity plots, displayed in Fig. 8. The scattering plots for both T and L resemble those shown in Figure 4 of Ref. [5]. The atomic displacements d_α corresponding to the acoustic modes (inhomogeneous strain) in our analysis corresponds to the uniform shifts that Ref. [5] uses to model their data. Our results that the patterns are rather similar for both T and L cases implies that more than one kind of atomic displacements or structures could be used to model experimental results and that the stripe-like solutions for the inhomogeneity is consistent with the experimental observation.

7 Discussion & Summary

We have presented new experimental data on perovskite crystals which show diffuse temperature dielectric anomalies. We presented a Landau-type theory of this diffuseness by considering local stresses produced by inhomogeneities. In the case of PFT the principal finding is that the extrapolated Curie temperature T_{CW} is larger than T_m and coincides with the temperature T_η. Following the recently proposed idea describing alternating domains in a heterogeneous media consisted of a ferroelectric thin film having thin dead layers or an epitaxial film grown on a substrate [15, 19] we propose that similar (but, most likely, short-range and random) structures appear in relaxors below T_d. We provided a rigorous solution for an extended heterogeneous media, two ferroelectric slabs divided by dielectric interfacial layers, and obtained that this lamellar structure also must have alternating domains in the ferroelectric slabs. We showed that the contribution of the domain wall movements into the dielectric permittivity in such a system is governed by the relative ratio of the total width of the dielectric layers and does not depend on the distribution of the widths over the layers. We also computed strains, displacements and inelastic scattering intensity of such a domain structure which are in line with recent experiments [3, 4, 5, 20]. The assumption that there are only two main kinds of the regions, ferroelectric and dielectric, is consistent with the experimental finding showing the existence of two different transverse optical modes corresponding to a two-band structure of heterogeneous binary compounds [3].

The alternating domain structure proposed is consistent with many experiments. Indeed, for instance, the "waterfall phenomenon" [4, 20] could be related in this case to (nanoscale) domains, the domain size determines the critical wave vector below which the waterfall phenomenon is observed. The coupling between local strain and polarization in alternating domains leads to atomic displacements consistent with the inelastic scattering results [5] and the observation of strong interaction between acoustic and optical modes [3, 20]. A strong coupling between the ferroelectric fluctuations and domain wall fluctuations leads to strong damping of ferroelectric fluctuations below the critical wave vector.

We have shown that in the model of the domain structure considered the contribution of the domain walls movements into dielectric response is especially large in the case when the relative width of the dielectric layers in the direction of the field is small and it is consistent with the recent theoretical

result obtained for a ferroelectric thin film having dead layers [15]. The universal relaxation recently observed in PMN even at temperatures larger than T_m [21] can now be understood on the basis of the irreversible domain wall movements [22] (the movements of the domain walls until there exists an electric field without further restoration after switching the field off). The Debye-type relaxation of domain walls is expected in the cases when there is a strong restoring field and this is also consistent with the existence of a strong dispersion at T_m [12, 22, 23]. The dielectric permittivity can now be found on the basis of the theory considering the phonons coupled to relaxators [24, 25, 26, 27]. This coupling in addition to the domains' freezing can explain the experimentally evidenced deviation from the Arrhenius law [25, 26, 27]. Some contribution to the dielectric permittivity from the Maxwell-Wagner mechanism is also possible.

Formation of the proposed alternating domain structure is not hampered by the depolarization field which is unfavorable for the formation of lone polar regions in a dielectric media [28]. The cooperative appearance of the alternating polar regions make them energetically more favorable than the lone separated polar regions [15]. We should stress that the lone polar regions (for example in chemical clusters) can also exist and contribute to the dielectric permittivity in the presence of free electrons that compensate the depolarization fields [29]; the change of polarization in this case is caused by both the local ionic dipole reorientations [30] and by the compensating charge movements.

A picture emerging from the data analysis is the following. At T_d there appear precursors of the alternating nanodomain structure with a short range alternation of the local polarization. The maximal possible wave vector of this domain structure just corresponds to the critical wave vector seen in the "waterfall" phenomenon [4, 20]. The dielectric permittivity of relaxors is high due to the large ferroelectric fluctuations and due to domain walls movements (see also [22, 23, 28, 31, 32]). At some temperature, known as the freezing temperature, the nanodomains become very large most probably due to the polarization percolation [12] and are frozen thereafter or a ferroelectric phase transition can take place. This scenario seems to be valid in the case of PMN and other classic relaxor materials as well.

In the case of NaNbGd T_{CW} lies below T_m, and the presence of the diffused temperature dielectric permittivity maximum, in our opinion, is due to the local stresses and local fields produced by the Gd impurities. The large difference between T_η and T_{CW} in this case hints that the new order param-

eter appearing at T_η has nothing to do with ferroelectric domain structure, also resulting in much smaller permittivity.

8 Acknowledgements

The authors appreciate discussions with Gehring, Shirane, Bokov, and Bratkovskiy. The study has been partially supported by RFBR grants 01-02-16029 and 01-03-33119.

Appendix A

The Poisson equation inside each of the slabs can be written in the form

$$\begin{array}{l}\varphi''_{1x}+\varphi''_{1y}+\varphi''_{1z}=0;\ \ \varphi''_{5x}+\varphi''_{5y}+\varphi''_{5z}=0;\ \ \varphi''_{3x}+\varphi''_{3y}+\varphi''_{3z}=0;\\ \varepsilon_{2x}\varphi''_{2x}+\varepsilon_{2y}\varphi''_{2y}+\varepsilon_{2z}\varphi''_{2z}=0;\varepsilon_{2x}\varphi''_{4x}+\varepsilon_{2y}\varphi''_{4y}+\varepsilon_{2z}\varphi''_{4z}=0.\end{array} \tag{8}$$

Here $\varepsilon_1, \varepsilon_3$ are the dielectric permittivities in the dielectric layer at the boundary of the system and in the middle respectively; $\varepsilon_{2z}, \varepsilon_{2x}, \varepsilon_{2y}$ are the dielectric permittivities in the ferroelectric slab in the corresponding directions; φ_i is the potential in the i-th slab, $\varphi'_{i\alpha}$ and $\varphi''_{i\alpha}$ are the first and the second derivatives with respect to α. The boundary conditions between the slabs at the voltage U are:

$$\begin{array}{l}\varepsilon_{2z}\varphi'_{2z}(-f/2)-\varepsilon_1\varphi'_{1z}(d_0)=-4\pi\sigma;\ \ \varepsilon_3\varphi'_{3z}(-d/2)-\varepsilon_{2z}\varphi'_{2z}(f/2)=4\pi\sigma\\ \varepsilon_{2z}\varphi'_{4z}(-f/2)-\varepsilon_3\varphi'_{33z}(d/2)=-4\pi\sigma;\ \ \varepsilon_1\varphi'_{5z}(d_0)-\varepsilon_{2z}\varphi'_{41z}(f/2)=4\pi\sigma\\ \varphi_1(0)=-U/2;\ \ \varphi_1(d_0)=\varphi_2(-f/2);\ \ \varphi_2(f/2)=\varphi_3(-d/2);\\ \varphi_3(d/2)=\varphi_4(-f/2);\ \ \varphi_4(f/2)=\varphi_5(d_0);\ \ \varphi_5(0)=U/2\end{array} \tag{9}$$

where the general solutions are given by [33]

$$\varphi_1(z,q_x,q_y) = C_{11}\frac{\sinh k_1 z}{\sinh k_1 d_0} + C_{12}\frac{\cosh(k_1 z)}{\cosh(k_1 d_0)}\ 0 < z < d_0$$
$$\varphi_2(z_2,q_x,q_y) = C_{21}\frac{\sinh(k_2 z_2)}{\sinh(k_2 f/2)} + C_{22}\frac{\cosh(k_2 z_2)}{\cosh(k_2 f/2)},\ \ -f/2 < z_2 < f/2$$
$$\varphi_3(z_3,q_x,q_y) = C_{31}\frac{\sinh(k_3 z_3)}{\sinh(k_3 d/2)},\ \ -d/2 < z_3 < d/2$$
$$\varphi_4(z_4,q_x,q_y) = C_{41}\frac{\sinh(k_2 z_4)}{\sinh(k_2 f/2)} + C_{42}\frac{\cosh(k_2 z_4)}{\cosh(k_2 f/2)},\ \ -f/2 < z_4 < f/2$$
$$\varphi_5(z_5,q_x,q_y) = C_{51}\frac{\sinh k_1 z_5}{\sinh k_1 d_0} + C_{52}\frac{\cosh(k_1 z_5)}{\cosh(k_1 d_0)},\ \ 0 < z_5 < d_0 \tag{10}$$

Here $z_2 = z + d_0 + f/2$, $z_3 = z_2 + f/2 + d/2$. The interfacial charge can be represented as a wave corresponding to alternating domains in the x and y directions placed in the checkboard (it is close to the honeycomb structure) or stripe-type style:

$$\sigma(x,y) = \sum_{q_x,q_y} \sigma(q_x,q_y) e^{q_x x + q_y y}$$
$$\sigma = \frac{2P_s}{iq_x T_x}\left(1 - e^{iq_x a_{x1}}\right)\delta_{q_y 0},\ q_x \neq 0, \quad \textit{stripes} \tag{11}$$
$$\sigma = -\frac{4P_s}{q_x T_x q_y T_y}\left(1 - e^{iq_x a_{x1}}\right)\left(1 - e^{iq_y a_{1y}}\right),\ \ q_x^2 + q_y^2 \neq 0;\ \ \textit{checkboard}$$

Here P_s is the local polarization magnitude inside domains; at zero wave vector $\sigma = \sigma_0$ where σ_0 can be found from the equilibrium condition which we will derive below. The lengths of the domains in the $x$and $y$directions ($a_{\alpha 1}$ and $a_{\alpha 2}$ where $\alpha = x, y$ for polarization up and down, $T_\alpha = a_{\alpha 1} + a_{\alpha 2}$) depend on the electric field magnitude.

Above we considered only the case when the polarization in the ferroelectric slabs is parallel, as, in the antiparallel case, the energy of the system is larger. The solution of the above equations in this case has the following symmetry conditions: $C_{42} = -C_{22}$; $\quad C_{41} = C_{21}$; $C_{52} = -C_{12}$; $\ C_{51} = -C_{11}$. From the equality of the potentials at the interfaces (see conditions (A2)) one obtains: $C_{31} = -C_{21} - C_{22}$; $\quad C_{11} = -C_{21} + C_{22} - C_{12}$; $C_{12} = 0$ at $q_x^2 + q_y^2 \neq 0$ and $C_{12} = -U/2$ at $q_x^2 + q_y^2 = 0$. From the Poisson equations in (A2) we have $C_{21}F_1 - C_{22}F_2 - C_{11}G_0 = -4\pi\sigma$ and $C_{31}G_1 - C_{21}F_1 - C_{22}F_2 = 4\pi\sigma$, where

$G_0 = \varepsilon_1 k_1 \coth(k_1 d_0)$, $G_1 = \varepsilon_3 k_3 \coth(k_3 d/2)$, $F_1 = \varepsilon_{2z} k_2 \coth(k_2 f/2)$, $F_2 = \varepsilon_{2z} k_2 \tanh(k_2 f/2)$. Excluding $C_{31}$and C_{11} one has:$(F_1 + G_0)C_{21} - (F_2 + G_0)C_{22} = -4\pi\sigma - C_{12}G_0$, $-(F_1 + G_1)C_{21} - (F_2 + G_1)C_{22} = 4\pi\sigma$. Under these conditions we obtained the following solution (only one coefficient will be necessary for the Free energy calculation) for $q_x^2 + q_y^2 \neq 0$

$$C_{21} = -\frac{4\pi\sigma\,(2F_2 + G_0 + G_1)}{(F_1 + G_0)(F_2 + G_1) + (F_1 + G_1)(F_2 + G_0)} \tag{12}$$

and for $q_x^2 + q_y^2 \to 0$:

$$C_{21} = \left(-4\pi\sigma\frac{L_g}{\varepsilon_g} + U\right)\frac{\varepsilon_t f}{2\varepsilon_{2z} L} \tag{13}$$

Here $L/\varepsilon_t = L_g/\varepsilon_g + L_f/\varepsilon_{2z}$, $L_g/\varepsilon_g = d/\varepsilon_3 + 2d_0/\varepsilon_1$, $L_f = 2f$.

The k_1, k_2 and k_3 can be found from the Poisson equations: $k_1^2 = k_3^2 = q_x^2 + q_y^2$, $\varepsilon_{2z} k_2^2 = \varepsilon_{2x} q_x^2 + \varepsilon_{2y} q_y^2$. Finally one obtains the Free energy in the form:

$$F = F_0 - 2S\sum_{q_x, q_y} C_{21}\sigma(q_x, q_y) - \frac{S\varepsilon_t U^2}{8\pi L} \tag{14}$$

where S is the surface area covered by the domains. The first term includes the Landau expansion with respect to polarization, domain wall energy and the energy connected with the appearance of polarization under the bias field; the second term describes the electrostatic energy of the boundaries; and the last term describes the capacitor energy due the bias field.

From (14) the macroscopic field energy (the terms corresponding to $q_x^2 + q_y^2 = 0$) can be represented in the form

$$f_M = F_M/LS = f_{M0} + \tfrac{1}{2}A\sigma_0^2 - E^*\sigma_0 \tag{15}$$

where $f_{M0} = \varepsilon_t U^2/8\pi L^2$, $A = 8\pi L^{-1}\left(\varepsilon_{2z}/L_f + \varepsilon_g/L_g\right)^{-1}$, $E^* = \varepsilon_t L_f U/\varepsilon_{2z} L^2$.

The alternating domain period can be now found from the equilibrium condition for the alternating field contribution to the Free energy

$$F_{alt} = \frac{Nf\Delta SP_s^2}{a} + \sum_{q_x^2+q_y^2\neq 0} \frac{8\pi S\sigma^2\left(2F_2+G_0+G_1\right)}{\left(F_1+G_0\right)\left(F_2+G_1\right)+\left(F_1+G_1\right)\left(F_2+G_0\right)} \tag{16}$$

where N =4 in the case of the checkboard order ($a = a_{x1} = a_{x2} = a_{y1} = a_{y2}$) and N =2 in the case of the striped domains ($a = a_{x1} = a_{x2}$; $a_{y1} = a_{y2} = \infty$); Δ is the characteristic domain wall width.

Especially simple solution can be obtained in the case when the dielectric and ferroelectric layers are thick in comparison with the domain width [15,34] and $\varepsilon_{2x} = \varepsilon_{2y}$:

$$a = \sqrt{\frac{Nf\Delta\left(\varepsilon_{2g}+\varepsilon_1\right)\left(\varepsilon_{2g}+\varepsilon_3\right)}{64\xi\left(2\varepsilon_{2g}+\varepsilon_1+\varepsilon_3\right)}} \tag{17}$$

where $\varepsilon_{2g} = \sqrt{\varepsilon_{2z}\varepsilon_x}$; ξ does not depend on $a$and for the checkboard order we have:

$$\frac{\pi^4\xi}{4} = \sum_{i=0}^{\infty}\sum_{j=0}^{\infty} \frac{1}{\left(2i+1\right)^2\left(2j+1\right)^2\sqrt{\left(2i+1\right)^2+\left(2j+1\right)^2}} \approx 0.813 \tag{18}$$

In the case of the striped domains [34]

$$\frac{\pi^2\xi}{2} = \sum_{i=0}^{\infty} \frac{1}{\left(2i+1\right)^3} \approx 1.0518 \tag{19}$$

The domain width increases with dielectric permittivity and the thickness of the ferroelectric slab.

In the case of thin dielectric interfacial layers and comparatively thick ferroelectric slabs in the stripe-type order and at $\varepsilon_1 = \varepsilon_3 = \sqrt{\varepsilon_{2z}\varepsilon_{2x}}$, $d/2 = d_0$ the problem can be reduced to the case considered in Ref. [15], and the final result is

$$a = 0.95d\exp\left(0.4\frac{a_K^2}{d^2}\right) \tag{20}$$

where a_K is the Kittel domain size parameter which coincides with (17). This expression shows that the domains extremely rapidly grow when the relative size of the dielectric interfacial layers in the direction of field becomes thinner.

References

[1] G. A. Smolenskii, V. A. Bokov, V. A. Isupov, N. N. Krainik, R. E. Pasynkov and A. I. Sokolov, Ferroelectrics and related materials, Gordon and Breach Sci. Publishers, N.Y., 1984.

[2] L. E. Cross, Ferroelectrics **76**, 241 (1987).

[3] S. B. Vakhrushev and S. M. Shapiro, in Fundamental Physics of Ferroelectrics 2002, edited by R. E. Cohen (American Institute of Physics, Melville, NY, 2002).

[4] P. M. Gehring, S. Wakimoto, Z.-G. Ye, and G. Shirane, Phys. Rev. Lett. **87**, 277601-1 (2001).

[5] K. Hirota, Z.-G. Ye, S. Wakimoto, P. M. Gehring, and G. Shirane, Phys. Rev. B **65**, 104105 (2002).

[6] I. P. Raevski, V. G. Smotrakov, S. O. Lisitsina, S. M. Zaitsev and S. V. Selin, Izv. Akad. Nauk SSSR, Ser. Neorg. Mater. **21**,846 (1985) (In Russian). [English translation: *Inorganic Materials* **21**,734 (1985)].

[7] I. P. Raevski, V. V. Eremkin, V. G. Smotrakov, M. A. Malitskaya, S. A. Bogatina and L. A. Shilkina, Crystallogr. Repts, **47** (2002). (In press).

[8] S. Nomura, H. Takabayashi and T. Nakagawa, Jap. J. Appl. Phys. **7**, 600 (1968).

[9] W. Z. Zhu, A. Kholkin, P. Q. Mantas and J. L. Baptista, J. Europ. Ceram. Soc. **20**,2029(2000).

[10] F. Chu, I. M. Reaney and N. Setter , Ferroelectrics. 151, 343 (1994).

[11] A. Geddo Lehmann and P. Sciau , J. Phys.: Condens. Matter. **11**,1235 (1999).

[12] V. Ya. Shur, G. G. Lomakin, V. P. Kuminov, D. V. Pelegov, S. S. Beloglazov, S. V. Slovikovski, and I. L. Sorkin, Phys. Solid State **41**, 453 (1999).

[13] S. A. Prosandeev, V. S. Vikhnin and S. E. Kapphan, Eur. Phys. J. B **15**, 469 (2000).

[14] S. A. Ivanov, S. Eriksson, N. W. Thomas, R. Tellgren and H. Rundlof, J. Phys.: Condens. Matter. **13**,25 (2001).

[15] A. M. Bratkovsky and A. P. Levanyuk, Phys. Rev. Lett. **84**, 3177 (2000); *ibid* **86**, 3642 (2001).

[16] I. P. Raevski and S. A. Prosandeev, J. Phys. Chem. Sol. (in press).

[17] J. Sigman and D. P. Norton, H. M. Christen, P. H. Fleming, and L. A. Boatner, Phys. Rev. Lett. **88**, 097601-1 (2202).

[18] U. V. Waghmare, E. J. Cockayne and B. P. Burton, in preparation

[19] N. A. Pertsev and A. G. Zembilgotov, J. Appl. Phys. **78**, 6170 (1995).

[20] S. Wakimoto, C. Stock, R. J. Birgeneau, Z.-G. Ye, W. Chen, W. J. L. Buyers, P. M. Gehring, and G. Shirane, Phys. Rev. B **65**, 172105 (2002).

[21] A. A. Bokov, and Z.-G. Ye, Phys. Rev. B 66, 0641XX (2002).

[22] W. Kleemann, J. Dec, S. Miga, Th. Woike, and R. Pankrath, Phys. Rev. B **65**, 220101-1 (2002).

[23] V. Ya. Shur, E. L. Rumyantsev, E. V. Nikolaeva, and E. I. Shishkin, Appl. Phys. Lett. **77**, 3636 (2000).

[24] S. A. Prosandeev, W. Kleemann and J. Dec, J. Phys.: Condens. Matter **13**, 5957 (2001).

[25] S. A. Prosandeev, V. A. Trepakov, M. E. Savinov, L. Jastrabik and S. E. Kapphan, J. Phys.: Condens. Matter **13**, 9749 (2001).

[26] S. A. Prosandeev and V. A. Trepakov, JETP **94**, 419 (2002).

[27] S. A. Prosandeev, Phys. Sol. St., **43**, 1948 (2001).

[28] A. E. Glazunov and A. K. Tagantsev, J. Phys.: Condens. Matter **10**, 8863 (1998).

[29] S. A. Prosandeev, V. S. Vikhnin and S. E. Kapphan, J. Phys.: Condens. Matter **14**, 4407 (2002).

[30] S. A. Prosandeev, cond-mat/0207374.

[31] J. F. Scott, Rep. Progr. Phys. **42**, 1055 (1979).

[32] O. Kircher, G. Diezemann, and R. Bohmer, Phys. Rev. B **64**, 054103 (2001).

[33] E. Salje, Phase Transitions in Ferroelastic and Co-elastic Crystals, 1993, Cambridge University Press, Cambridge, UK

[34] C. Kittel, Phys. Rev. **70**, 965 (1946).

Figure captions

Figure 1. *ε'(T)* dependencies for the PFT crystal, measured at different frequencies.

Figure 2. Temperature dependencies of ε' (1) and $1/\varepsilon$' (2) measured at 10^6Hz for the PFT crystal. Curve 3 shows the difference between the experimental $1/\varepsilon$ dependence and the Curie-Weiss fit of $1/\varepsilon$. Straight solid lines are guides to the eye.

Figure 3. Temperature dependencies of ε' measured at 10^3, 10^4,10^5, 10^6Hz. for $0.88NaNbO_3$-$0.12Gd_{1/3}NbO_3$ crystal.

Figure 4. Temperature dependencies of ε and *1/*ε measured at 10^5Hz for $0.88NaNbO_3$-$0.12Gd_{1/3}NbO_3$ crystal and the difference between the experimental $1/\varepsilon$ dependence and the Curie-Weiss fit of $1/\varepsilon$. Straight solid lines are guides to the eye.

Figure 5. The fit of the model expression to the experimental data.

Figure 6. The model lamellar structure consisted of ferroelectric and dielectric slabs.

Figure 7.Contourplots of (a) atomic displacements $d_x(r)$, $d_y(r)$, (b) local strains $u_{xx}(r)$, $u_{yy}(r)$, (c) $u_{xy}(r)$ and local polarization $P_x(r)$ for the alternating domain-stripe solutions of the model inhomogeneous ferroelectric in 2-dimension.

Figure 8. Contourplot of the inelastic scattering intensity for the alternating domain-stripe solution discussed in Section 6.

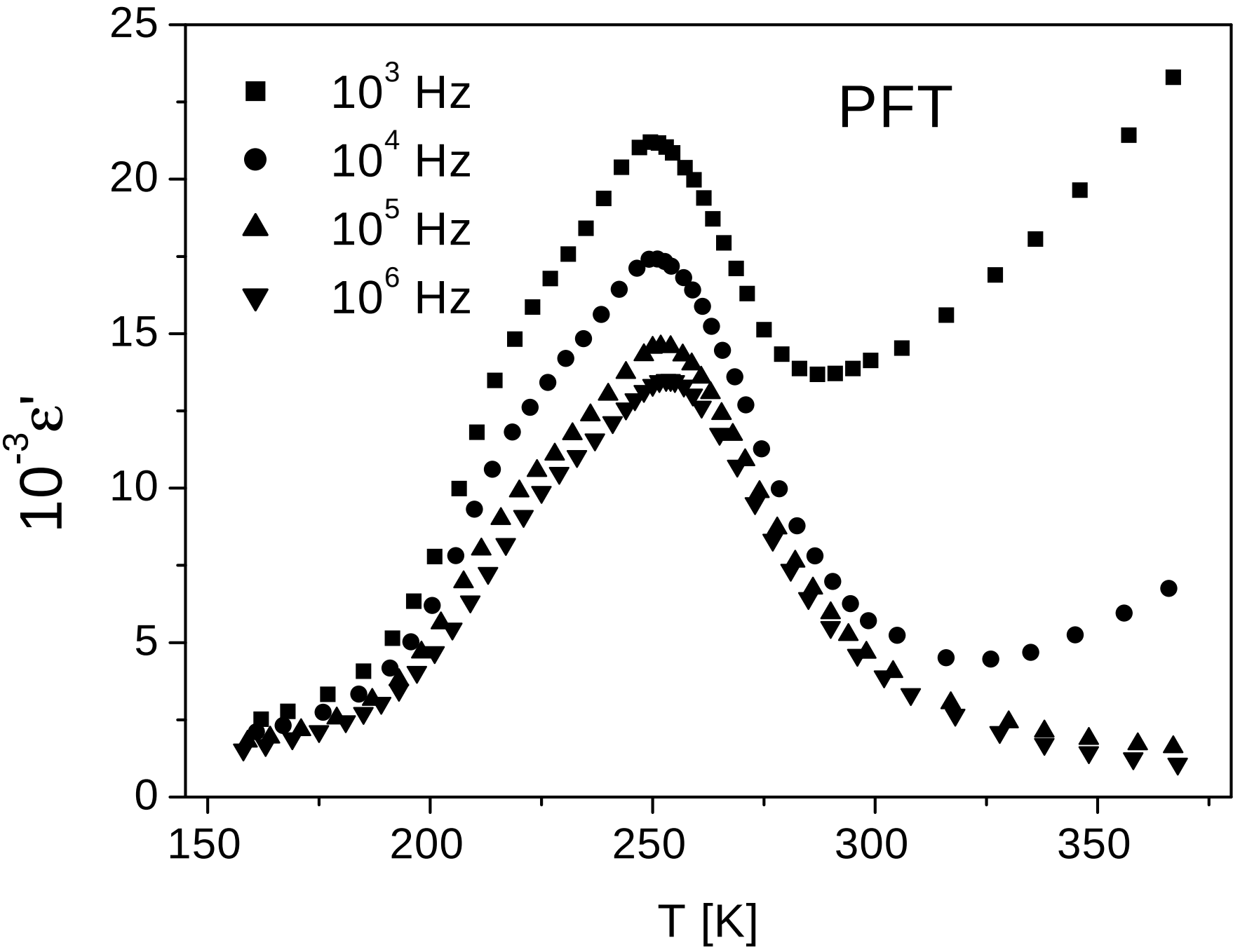
PFT
10^3 Hz
10^4 Hz
10^5 Hz
10^6 Hz
$10^{-3}\varepsilon'$
T [K]
0
5
10
15
20
25
150
200
250
300
350

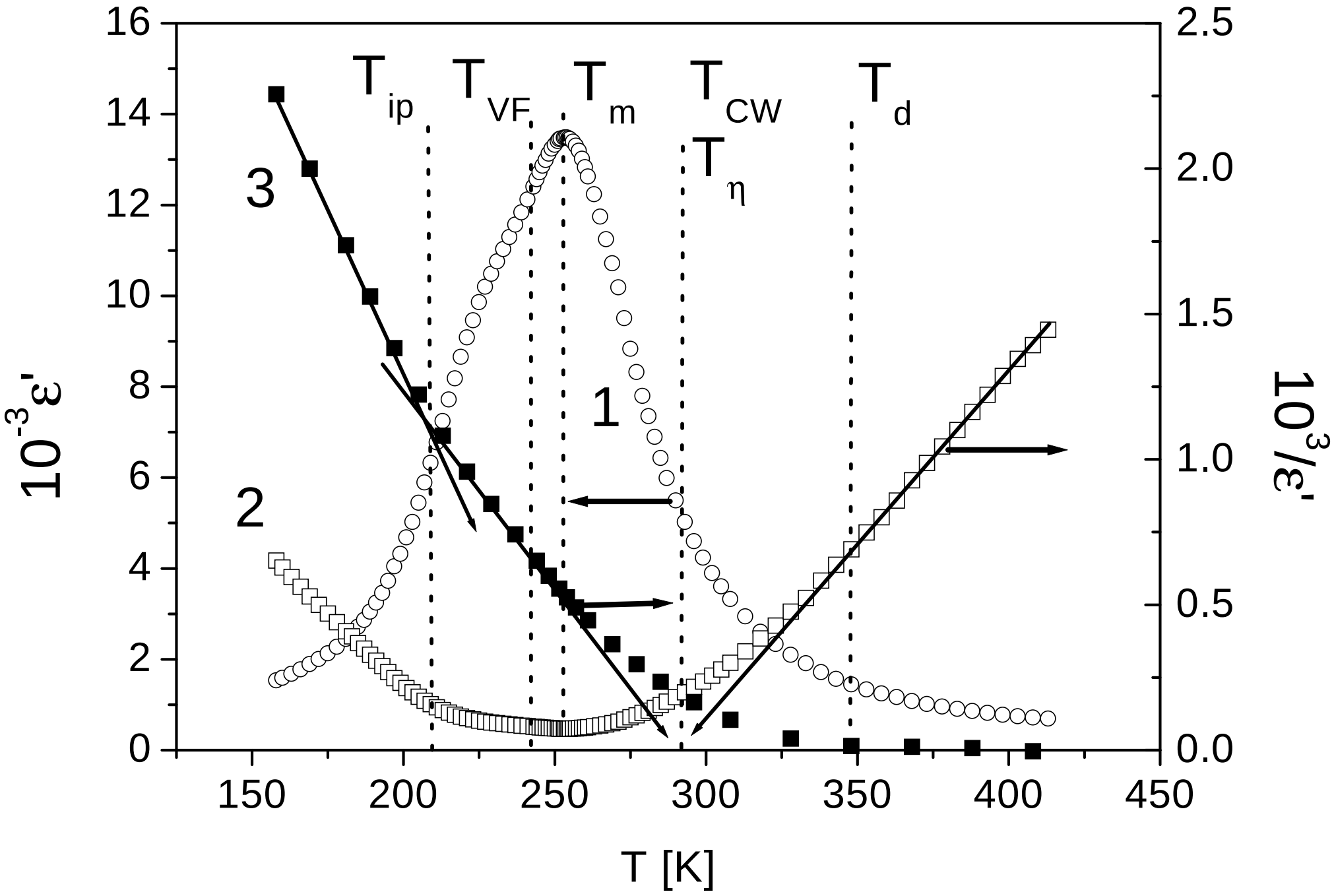
16
14
12
10
8
6
4
2
0
2.5
2.0
1.5
1.0
0.5
0.0
150
200
250
300
350
400
450
T [K]
10^-3 ε'
10^3/ε'
T_ip
T_VF
T_m
T_CW
T_η
T_d
1
2
3

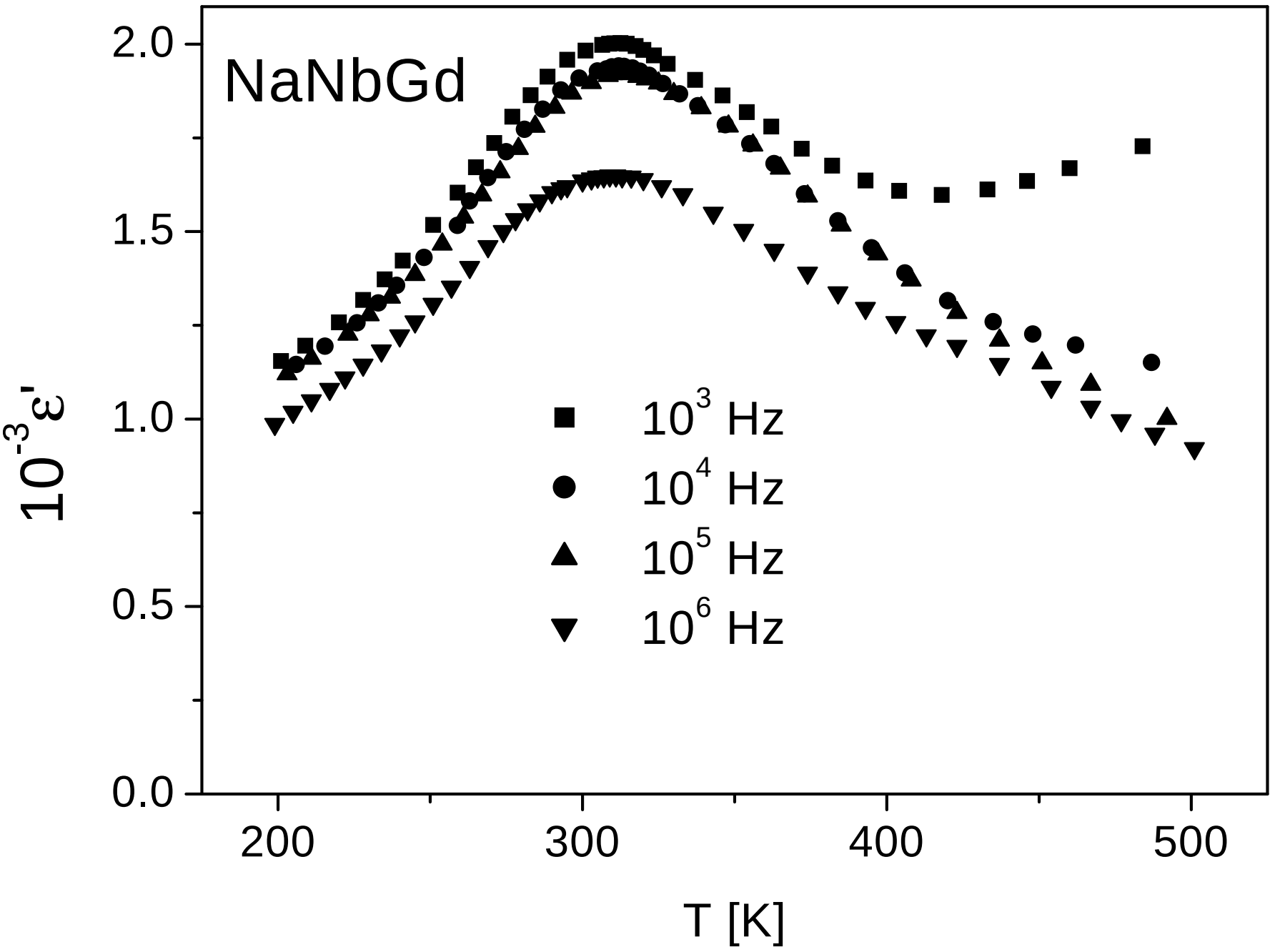
NaNbGd
2.0
1.5
1.0
0.5
0.0
200
300
400
500
T [K]
$10^{-3}\varepsilon'$
10^3 Hz
10^4 Hz
10^5 Hz
10^6 Hz

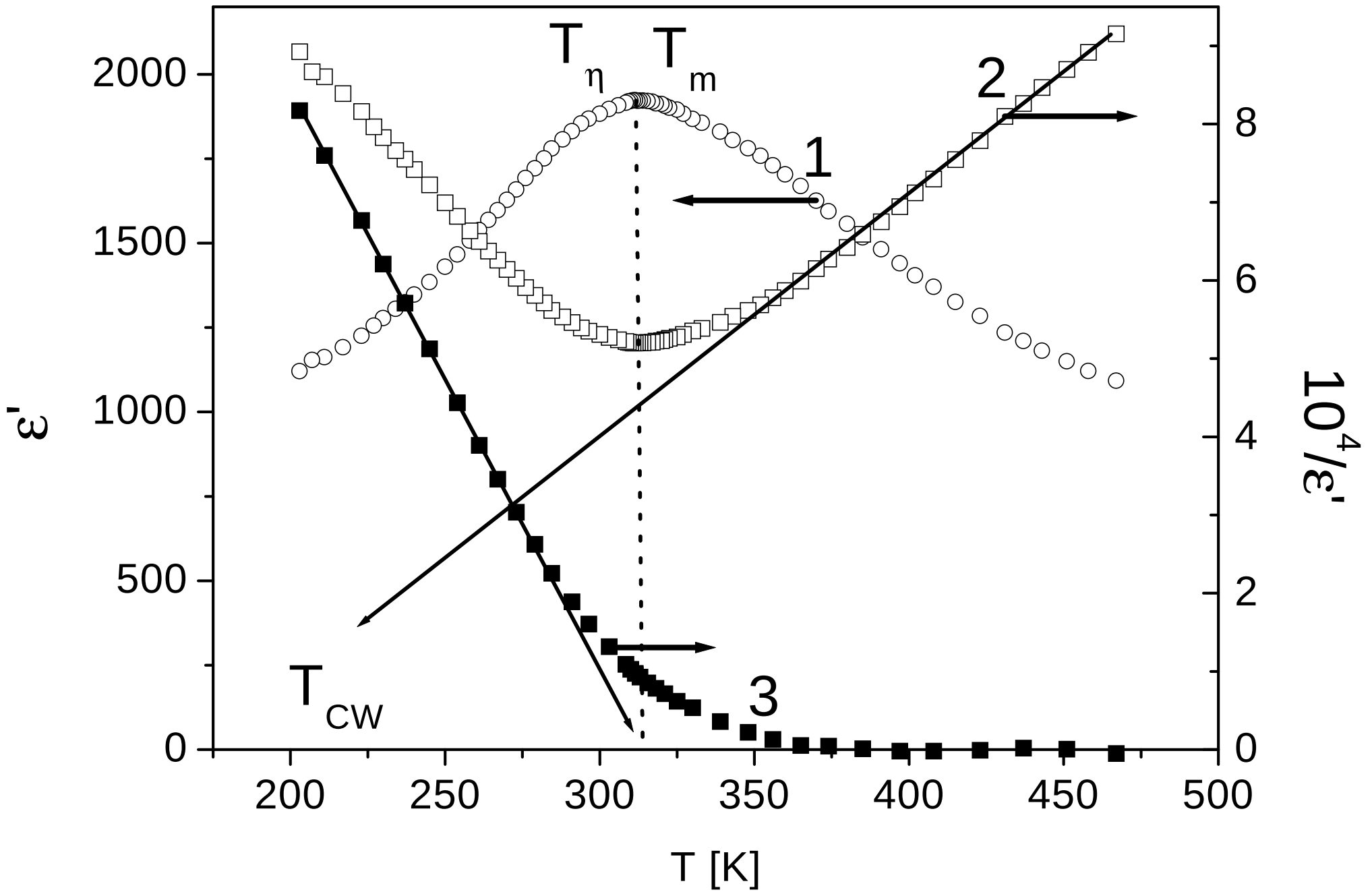
2000
1500
1000
500
0
ε'
200
250
300
350
400
450
500
T [K]
8
6
4
2
0
10⁴/ε'
T_η
T_m
T_CW
1
2
3

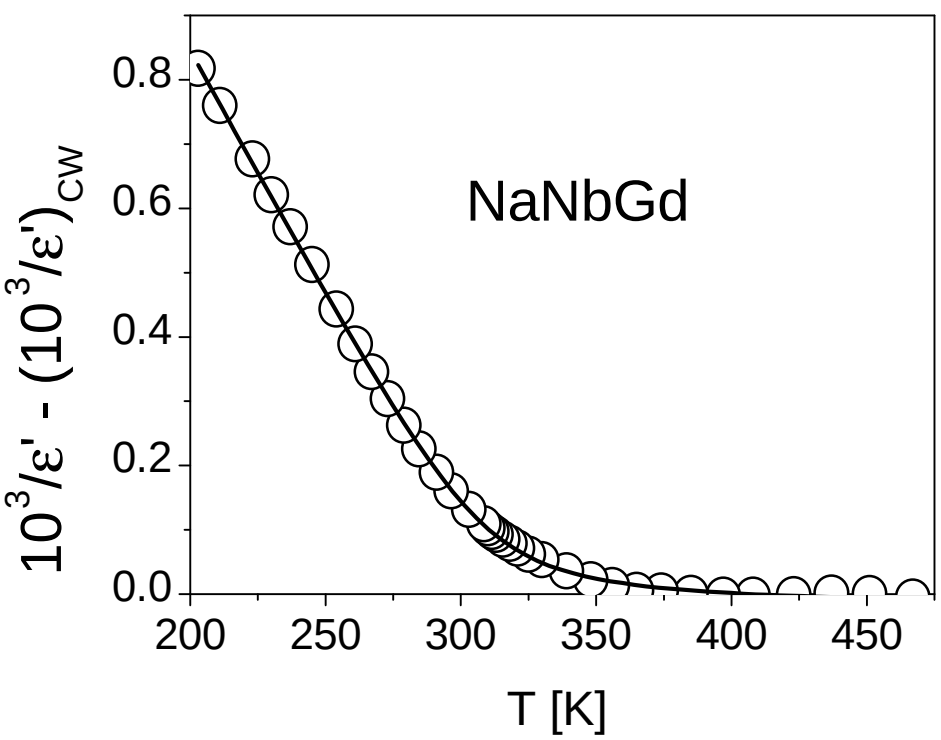
NaNbGd
$10^3/\varepsilon' - (10^3/\varepsilon')_{CW}$
T [K]
0.0
0.2
0.4
0.6
0.8
200
250
300
350
400
450

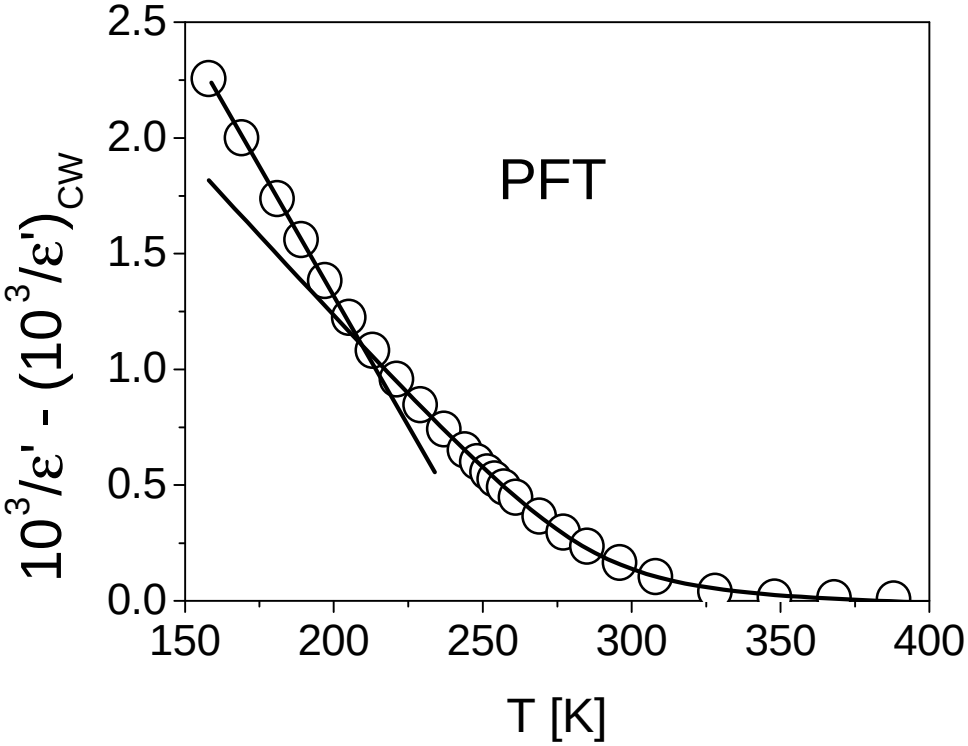
PFT
$10^3/\varepsilon' - (10^3/\varepsilon')_{CW}$
T [K]
0.0
0.5
1.0
1.5
2.0
2.5
150
200
250
300
350
400

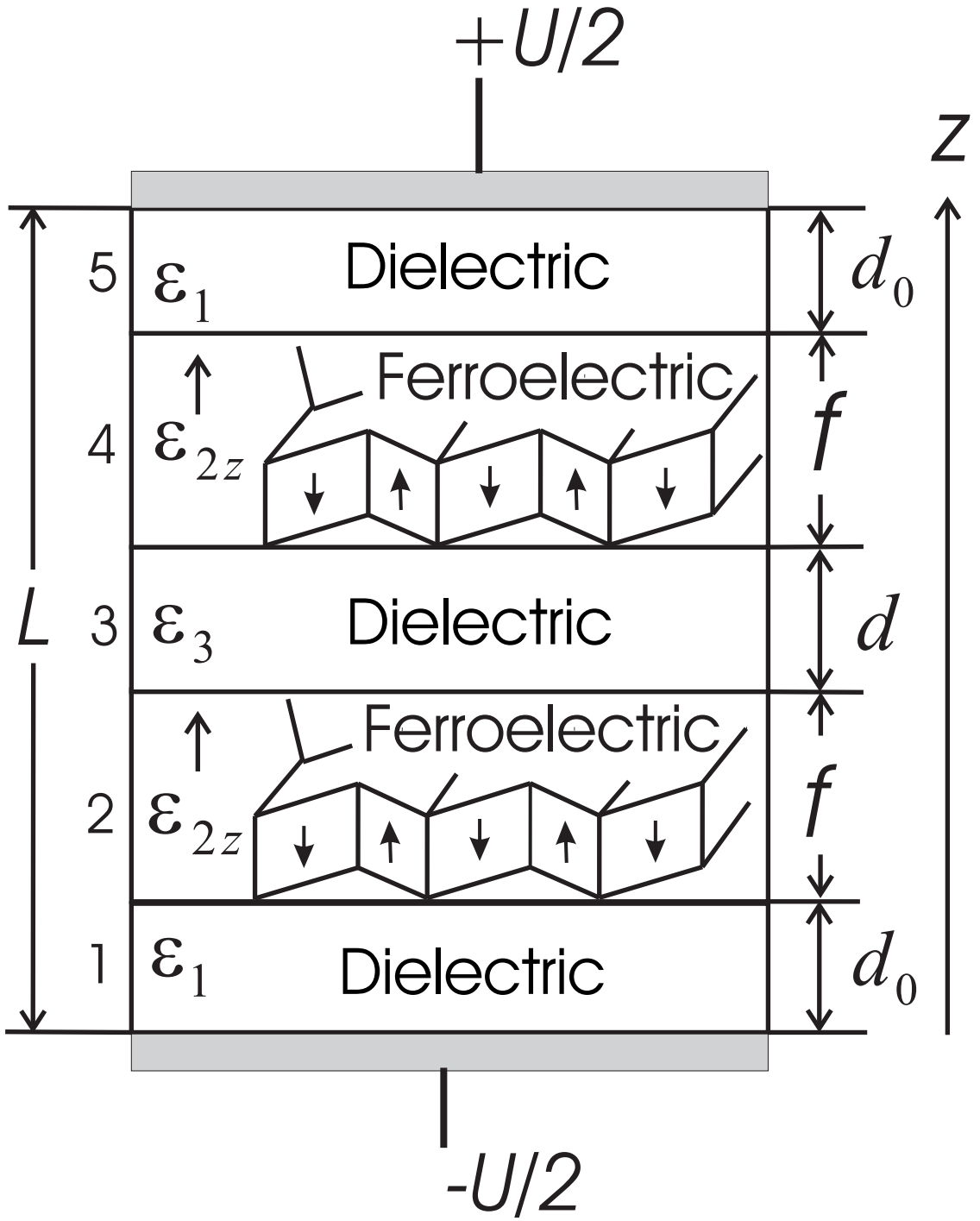
+U/2
z
5
ε1
Dielectric
d0
Ferroelectric
4
ε2z
f
L
3
ε3
Dielectric
d
Ferroelectric
2
ε2z
f
1
ε1
Dielectric
d0
-U/2

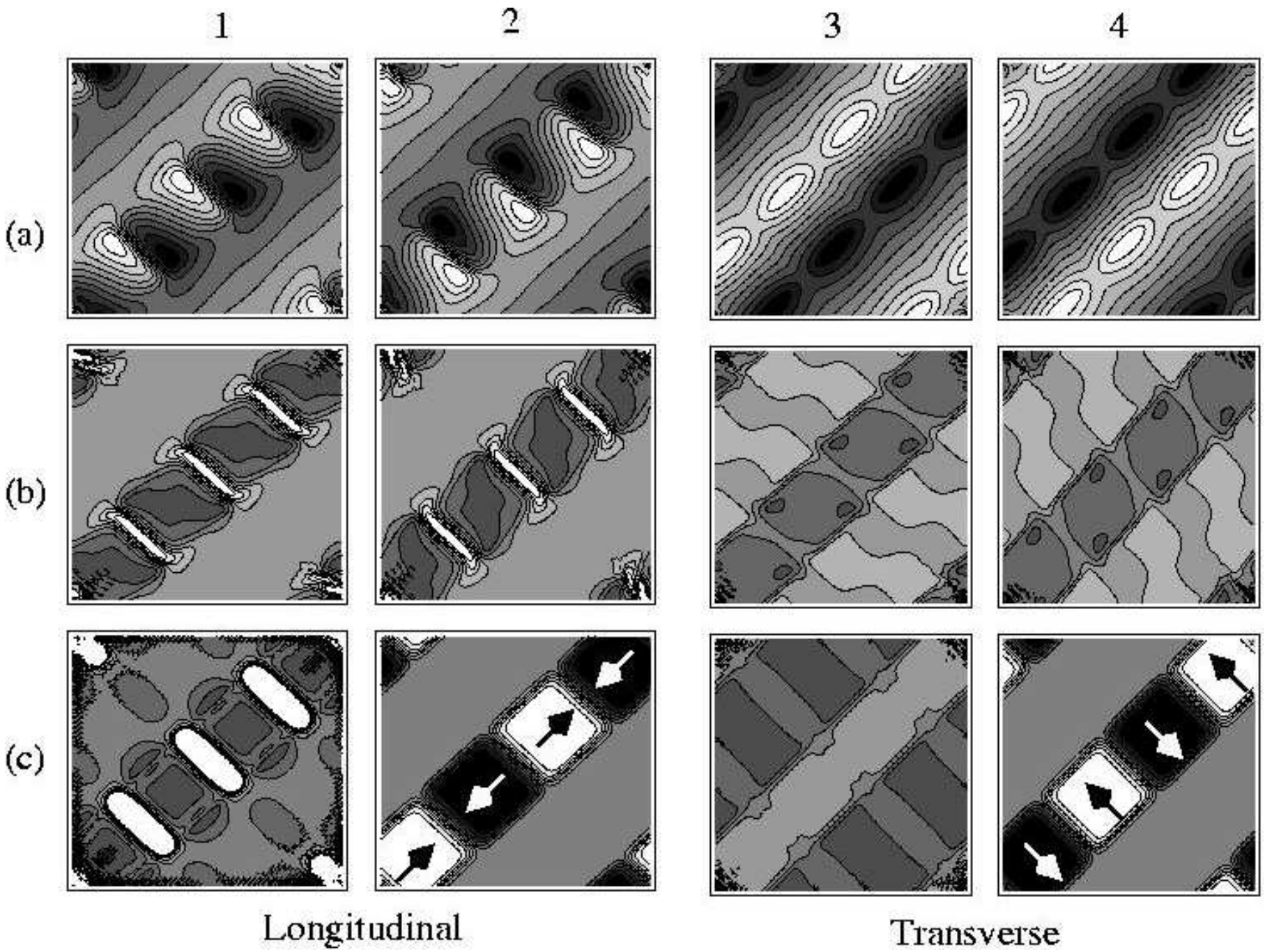
1
2
3
4
(a)
(b)
(c)
Longitudinal
Transverse

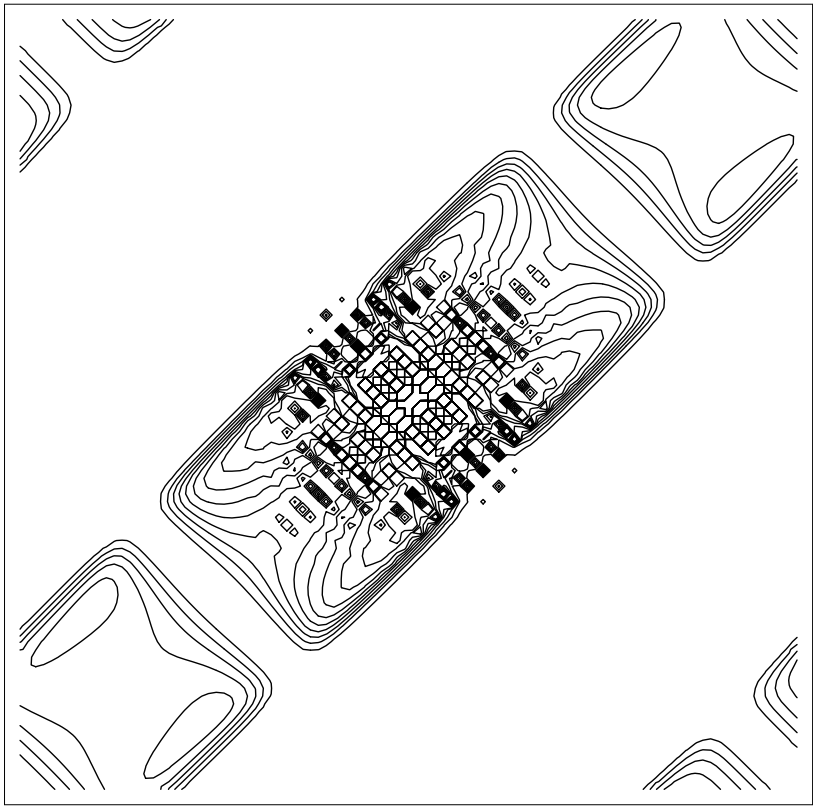

Longitudinal

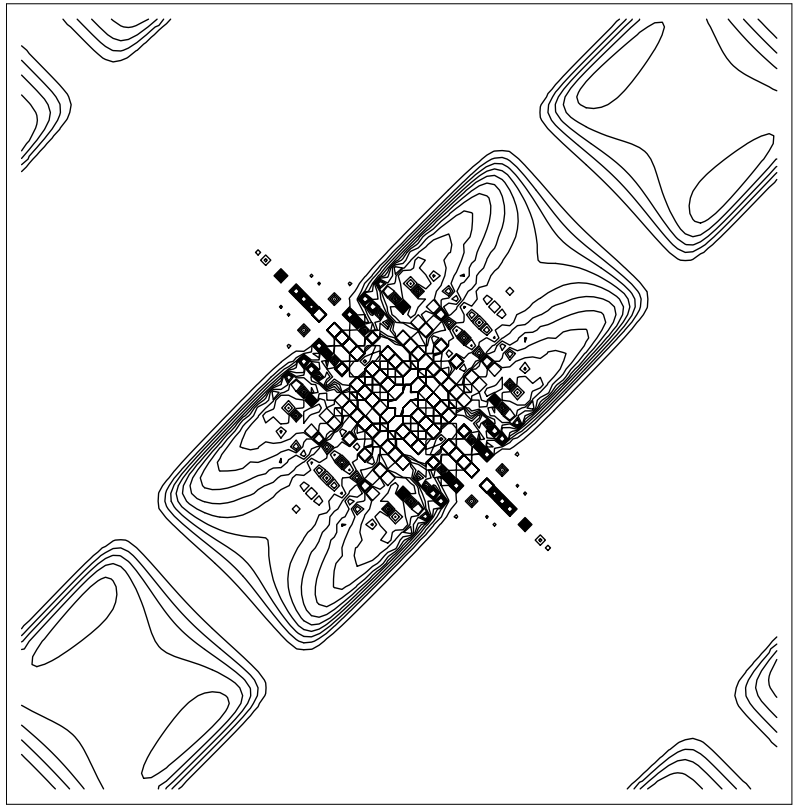

Transverse